Journal of Solid State Chemistry 242 (2016) 77–85

Contents lists available at ScienceDirect

Journal of Solid State Chemistry

journal homepage: www.elsevier.com/locate/jssc

Synthesis, characterization and electrocatalytic properties of delafossite $CuGaO_2$

Jahangeer Ahmed [a,b], Yuanbing Mao [a,*]

[a] Department of Chemistry, University of Texas Rio Grande Valley, 1201 West University Drive, Edinburg, TX 78539, United States
[b] Department of Chemistry, College of Science, King Saud University, Riyadh 11451, Saudi Arabia

ARTICLE INFO

Article history:
Received 21 April 2016
Received in revised form
1 July 2016
Accepted 4 July 2016
Available online 5 July 2016

Keywords:
$CuGaO_2$
Delafossite
Oxygen evolution reaction
Hydrogen evolution reactions
Electrocatalytic activity

ABSTRACT

Delafossite $CuGaO_2$ has been employed as photocatalysts for solar cells, but their electrocatalytic properties have not been extensively studied, especially no comparison among samples made by different synthesis routes. Herein, we first reported the successful synthesis of delafossite $CuGaO_2$ particles with three different morphologies, i.e. nanocrystalline hexagons, sub-micron sized plates and micron–sized particles by a modified hydrothermal method at 190 °C for 60 h [1–3], a sono-chemical method followed by firing at 850 °C for 48 h, and a solid state route at 1150 °C, respectively. Morphology, composition and phase purity of the synthesized samples was confirmed by powder X-ray diffraction and Raman spectroscopic studies, and then their electrocatalytic performance as active and cost effective electrode materials to the oxygen and hydrogen evolution reactions in 0.5 M KOH electrolyte versus Ag/AgCl was investigated and compared under the same conditions for the first time. The nanocrystalline $CuGaO_2$ hexagons show enhanced electrocatalytic activity than the counterpart sub-micron sized plates and micron-sized particles.

1. Introduction

Delafossite ternary oxides have an AMO_2-type general structure, where 'A' is monovalent (1+ metals like Cu, Ag, etc.) and 'M' is trivalent (3+ metals like Al, Ga, In, Fe etc.). Delafossite $CuMO_2$ with monovalent Cu ion has closed packed plane with edge sharing of MO_6 octahedra [4,5]. It belongs to a group of *p*-type transparent conducting oxides and has a band gap of 3.6 eV [6,7]. The *p*-type conductivity in delafossite compounds was first discovered by Kawazoe et al. in 1997 [8]. The conductivity and electronic structures of delafossite ($CuM^{III}O_2$) materials are reported in details elsewhere [1,9]. Delafossite $CuGaO_2$ demonstrates very interesting properties including optical [9,10], electronic [7,9,10], and photovoltaic properties [2,3,11]. $CuGaO_2$ nanoplates have been used as the photo-electrode materials in *p*-type dye sensitized solar cells to accelerate the photo-voltage and photocurrent [2,3]. Sub-micron sized $CuGaO_2$ particles were also used as photo-electrode materials in the H_2 generation by splitting of hydrogen sulfide [12] and photochemical reduction of CO_2 to CO [13]. Electrochemical impedance spectroscopy was employed to determine the hole conductivity and acceptor density of $CuGaO_2$ nanoparticles [14]. Other than studies on $CuGaO_2$, as the literature review points out, there were very few reports on the electrocatalysis of delafossite materials, e.g. $PtCoO_2$ [15], $PdCoO_2$ [15], $PdRhO_2$ [15], $CuRhO_2$ [16,17], $CuAlO_2$ [17,18], but not extensively, nor comparatively among different morphologies. Hinogami et al. have reported $CuRhO_2$ delafossite as active electrocatalysts for oxygen evolution reaction (OER) using 1.0 M KOH electrolyte and reversible hydrogen electrode as a reference electrode [17]. Copper based nanostructures including oxides [19] and intermetallic [20,21] have also been used as the electro-catalysts in hydrogen evolution reaction (HER) and OER using 0.5 M KOH electrolyte versus Ag/AgCl as a reference electrode. Therefore, delafossites with copper at the A-site have demonstrated significant electronic properties but their electrochemical studies are still lacking [8,14], which motivates us to study delafossite $CuGaO_2$ with different morphologies on their electrochemical performance to OER and HER.

Delafossite $CuGaO_2$ nanostructures are of great interest in electrolysis of water for oxygen and hydrogen evolutions. Renewable and clean energy is the most important challenge for scientists due to the declining non-renewable energy sources (i.e. coal and oil). Hydrogen is an important form of energy carrier for next generation fuel to run the world's economy and has higher energy content. Electrolysis of water for hydrogen and oxygen evolution has an immense potential to supply sustainable energy via fuel cells, battery devices etc. Hydrogen is also a clean fuel which can be used in the fuel cells by converting the chemical

* Corresponding author.
E-mail address: yuanbing.mao@utrgv.edu (Y. Mao).

http://dx.doi.org/10.1016/j.jssc.2016.07.006
0022-4596/

energy in to electrical energy. Hydrogen also combines with oxygen to produce electricity in a fuel cell. Oxygen could also be used in fuel cells in the generation of power by increasing the temperature of the reactor to complete the combustion of fuels. More specifically, the aim of the present work is to provide active and cost effective delafossite $CuGaO_2$ electro-catalysts for OER and HER. Oxygen and hydrogen are commonly used as fuels in power generations, automobile and aerospace industries. Here, we report that nanocrystalline $CuGaO_2$ hexagons show enhanced electrocatalytic activity as compared to the sub-micron sized and micron sized particles of $CuGaO_2$ counterparts for the OER and HER in 0.5 M KOH versus Ag/AgCl. The structural and morphological characterizations of the materials were investigated by powder x-ray diffraction (PXRD), Raman spectroscopy, thermo-gravimetric analysis, energy dispersive studies and electron microscopic studies. The electrochemical studies were successfully carried out using three electrode based electrochemical work station. The electrolysis of water by using the synthesized delafossite $CuGaO_2$ catalysts shows a clear feasibility of current generation in alkaline electrolyte. Besides, these delafossite $CuGaO_2$ materials could be useful to sustain the energy through fuel cells, battery devices, electrolyzer, solar water splitting, etc.

2. Experimental section

2.1. Materials and methods

The following reagents were used in the synthesis of $CuGaO_2$ delafossites: $Cu(NO_3)_2 \cdot 3H_2O$ (Sigma Aldrich, 99%), $Ga(NO_3)_3 \cdot xH_2O$ (Alfa Aesar, 99.9%), PEG 20,000 (Polyethylene glycol) (Alfa Aesar), ethylene glycol (Alfa Aesar, 99%), KOH (JT Baker Chemical Company), $NaHCO_3$ (Sigma Aldrich, 99.7%), and ethanol (Alfa Aesar, 96%). Thermal analysis of the commercial $Ga(NO_3)_3 \cdot xH_2O$ produces a mass loss of ~74%, which corresponds to loss of six water molecules as reported. [22] Therefore, we have used six water molecules of $Ga(NO_3)_3 \cdot xH_2O$ in our experiments to maintain the stoichiometric ratio of 1:1 of Cu:Ga.

2.2. Hydrothermal synthesis of nanocrystalline $CuGaO_2$ hexagons

Nanocrystalline delafossites $CuGaO_2$ hexagons were synthesized using the modified hydrothermal method [1–3]. An appropriate stoichiometric mixture of copper and gallium precursors in the molar ratio of 1:1, i.e. 0.002 mol of $Cu(NO_3)_2 \cdot 2.5H_2O$ and 0.002 mol of $Ga(NO_3)_3 \cdot 6H_2O$, was added into a 100 ml Teflon vessel. Subsequently, 10 ml of deionized water, 10 ml of absolute ethanol, 5 ml of ethylene glycol and 100 mg of PEG 20,000 were added into the vessel. Then 15 ml of 0.5 M KOH solution was added to the autoclave containing the resulting mixture (pH ~8) and kept at 190 °C for 60 h. A mixture of ethanol and water has been used as a solvent in the hydrothermal process. The surface tension of ethanol (22.39 mN/m) is lower than water (77.82 mN/m) at room temperature. High surface tension of the solvent would lead agglomeration of the particles. Addition of ethanol in water decreases the surface tension of the solvent that could help to increase the reaction kinetics of $CuGaO_2$ particles and decrease the agglomeration of the particles. The resulting products were washed with ammonia and dilute nitric acid followed by washing with deionized water. Finally a light yellow colored powder was collected and dried at 70 °C for 4 h.

2.3. Sono-chemical synthesis of sub-micron sized $CuGaO_2$ plates

The sono-chemical synthesis involved the mixing of parent materials (0.03 M $Cu(NO_3)_2 \cdot 3H_2O$ and 0.03 M $Ga(NO_3)_3 \cdot xH_2O$) followed by titration with 0.15 M $NaHCO_3$ solutions drop by drop at 25 °C under ultrasonic process and kept for 3 h. The light green precipitates were collected by centrifugation and washed with deionized water three times. The resulting products were then dried at 60 °C for 6 h and used as the precursor materials in the synthesis of the delafossite $CuGaO_2$ sub-micron sized plates by annealing the above precursor at 850 °C for 48 h under ultra-pure nitrogen (99.999%) flow to form gray colored $CuGaO_2$ plates.

2.4. Solid state route of synthesis of micron-sized $CuGaO_2$ particles

Micron-sized $CuGaO_2$ particles were synthesized via solid state route. Gallium oxide (Ga_2O_3, Sigma Aldrich, 98%) and copper oxide nanopowder (CuO, Sigma Aldrich, size ~50 nm) were taken in 1:2 M ratio and ground together in an agate mortar pestle for 30 min. The resulting precursor was then annealed at 1150 °C for 36 h under N_2 gas flow.

2.5. Characterizations

All the resulting products were initially characterized by PXRD to determine the phase purity of the obtained delafossite $CuGaO_2$ samples using a Bruker D8 Advanced diffractometer with Ni-filtered Cu-K_α radiation at a scan speed of 1 s and scan step of 0.02° on a zero background sample holder. Raman scattering data was collected on a Bruker SENTERRA RAMAN microscope with an objective of 20X of optical microscope. The excitation line (785 nm) of an Ar^+ laser beam was focused to a spot size of 5 μm with a laser power of 10 mW. The spectral resolution range was used 3–5 cm^{-1} with the integration time of 100 s. Electron microscopic studies were carried out with a ZEISS SIGMA VP field emission scanning electron microscope (FESEM) operated at 5 kV. Transmission electron microscopic (TEM) studies were carried out with a ZEISS LEO 900 electron microscope operated at 80 kV. TEM specimens for the measurements were prepared by dispersing the delafossite $CuGaO_2$ powder samples in ethanol via ultra-sonication, a drop was put onto a porous carbon film supported by a copper grid, and then dried in air. Thermo-gravimetric analysis (TGA) was carried out using a Perkin-Elmer system with a heating rate of 5 °C/min in oxygen atmosphere.

2.6. Preparation of electrode materials and electrochemical measurements

The electrochemical studies were carried out with a computer controlled potentiostat/galvanostat electrochemical work station (Metrohm Autolab B.V.) at room temperature. Three electrodes (Pt wire, Ag/AgCl, and glassy carbon electrodes as the counter electrode, reference electrode and working electrode, respectively) were used in the electrolysis of water to OER and HER. The working electrodes were prepared by pasting slurries of the $CuGaO_2$ powders mixed with carbon black and PVDF (weight fractions of $CuGaO_2$:carbon black:PVDF of 75:15:10) on the surface of glassy carbon electrode. PVDF (polyvinylidene difluoride) was used as a binder with carbon black as conductive additive in the preparation of electrode materials. The prepared electrodes were then dried at 65 °C for overnight in vacuum oven and used as a working electrode for the electrochemical measurements. Cyclic voltammetry (CV) was carried at the scan rate of 50 mV/s with a peak window between from –1.0 to 1.1 V versus Ag/AgCl electrode in 0.5 M KOH electrolyte. Electrolyte solution of 0.5 M KOH(*aq*) versus Ag/AgCl electrode (reference electrode) has been used in present electrochemical studies according to the literature [18–21]. Chronoamperometric measurements were carried out for 200 s at 0.60 V and − 1.2 V versus Ag/AgCl for OER and HER, respectively, in 0.5 M KOH electrolyte. Carbon corrosion at a high potential is

largely responsible to ruin the OER performances. Therefore, to avoid the carbon corrosion, we have studied the oxygen evolution reactions (OER) at low potential (0.60 V) using chronoamperometry. Nitrogen gas was purged through the electrolyte for 5 min prior to the electrochemical measurements to remove dissolved air from the electrolyte toward the OER and HER. Also electrochemical measurements were run in O_2-saturated 0.5 M KOH for OER. Note that freshly prepared electrodes and electrolytes were used in each measurement for the OER and HER studies. The current density of the $CuGaO_2$ electro-catalysts was calculated using the surface area, amount of catalysts pasted on the glassy carbon and generated current.

3. Results and discussion

Using the sono-chemical method, crystalline sub-micron sized $CuGaO_2$ plates were synthesized after annealing the precursor materials prepared at 25 °C in N_2 atmosphere at 850 °C. Fig. 1a shows the PXRD pattern of the green colored precursors obtained from the sono-chemical method showing the crystalline phases of basic copper carbonate ($Cu_2(OH)_2CO_3$) and gallium hydroxide ($Ga(OH)_3$). This green colored precursor was converted into gray colored $CuGaO_2$ powder with rhombohedral crystal structure (Fig. 1b) after fired at 850 °C for 48 h under N_2 gas flow. As reported in the literature, $CuGaO_2$ is thermodynamically unstable at or below 1100 °C and 1200 °C in nitrogen and air, respectively [23,24]. Phase pure nanocrystalline $CuGaO_2$ hexagons in light yellow color were synthesized using the modified hydrothermal methods at 190 °C (Fig. 1c). All the observed reflections from the PXRD studies could be indexed with the peaks of (003), (006), (101), (012), (104), (015) and (018) on the basis of rhombohedral unit cell with the space group R-3 m (JCPDS file # 00-035-1402). Fig. 1d shows the pure phase of micron-sized $CuGaO_2$ particles obtained at 1150 °C for 36 h in N_2 via the solid state route. Fig. 1d shows narrower XRD pattern of the $CuGaO_2$ particles obtained at 1150 °C via solid state route as compared to the other two $CuGaO_2$ samples (Fig. 1d vs c and b). This could be possible because the crystalline size of the three $CuGaO_2$ samples increases with processing temperatures. The temperature of the synthesis reaction, the nature of the reactants and the way of the preparation of materials play crucial roles in the formation of materials. Therefore, Bragg's reflections of the (*hkl*) depend on the crystallinity and size of the obtained samples.

Moreover, Raman spectra of these nanocystalline hexagons, sub-micron sized plates and micron-sized particles of $CuGaO_2$ were collected by employing normal backscattering geometry as shown in Fig. 2. For the sub-micron sized $CuGaO_2$ plate sample, three characteristic Raman bands are identified at 203, 362 and 730 cm^{-1}, assigned to the A_g, E_g, and $A_{1\,g}$ modes of rhombohedral structure, respectively, which agree well with that of the reported delafossite $CuGaO_2$ [25,26]. All these three Raman bands of A_g, E_g, and A_{1g} also appear with nanocrystalline $CuGaO_2$ hexagons and micron-sized particles at 204, 367 and 737 cm^{-1}, respectively. The A_g and A_{1g} phonon modes denote the atomic vibrations in the direction of c-axis along the O–Cu–O bonds while the E_g mode

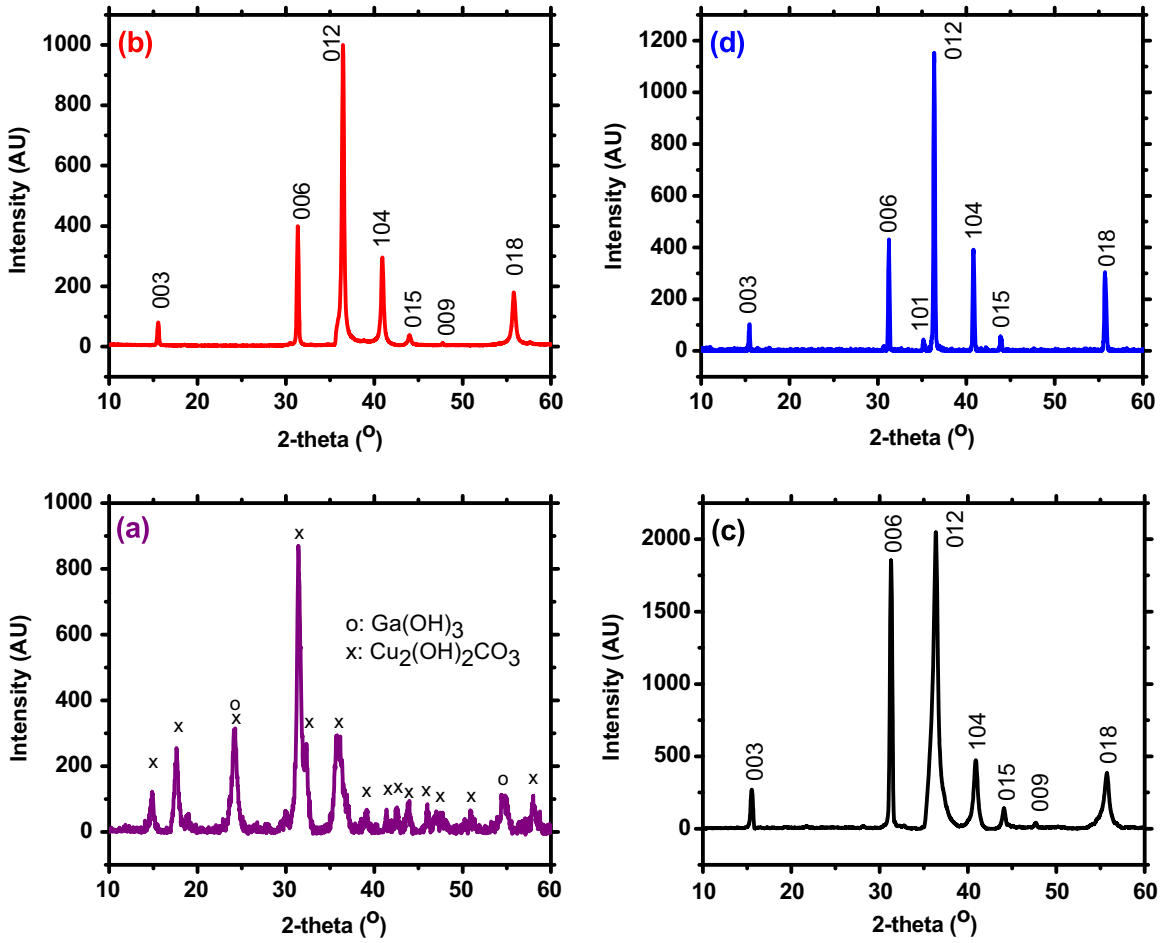

Fig. 1. PXRD patterns of (a) the as-synthesized precursor by the sono-chemical method; (b) the sub-micron sized $CuGaO_2$ plates obtained by firing the sono-chemical precursor at 850 °C for 48 h in N_2; (c) the nanocrystalline $CuGaO_2$ hexagons obtained by the hydrothermal method at 190 °C for 60 h; (d) the micron-sized $CuGaO_2$ particles obtained by solid state route at 1150 °C for 36 h in N_2.

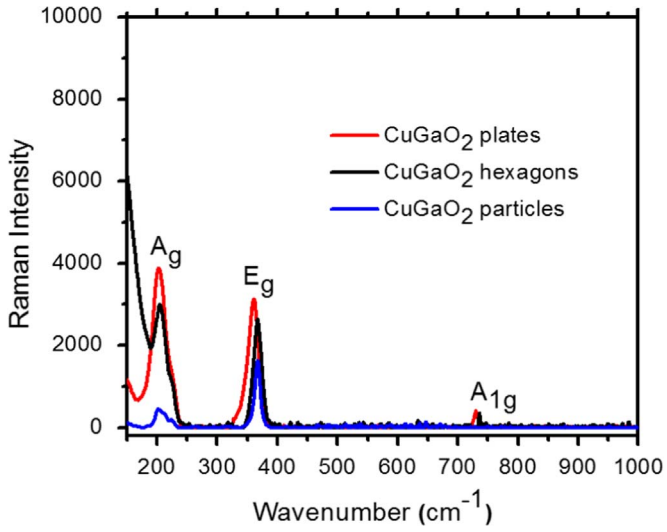

Fig. 2. Raman spectra of the nanocrystalline $CuGaO_2$ hexagons, sub-micron sized $CuGaO_2$ plates, and micron-sized $CuGaO_2$ particles.

(double degenerate) describes the vibration in the perpendicular direction along the c-axis. A small shift in the Raman peak positions of E_g and A_{1g} phonon modes to the higher wavenumbers was observed when comparing the nanocrystalline $CuGaO_2$ hexagons and micron-sized particles with the sub-micron sized $CuGaO_2$ plates. This small shift in the E_g and A_{1g} phonon modes (Raman active mode) could be due to the surface effects or disorder in the powder with pressure [26].

The microscopic studies by FESEM show the formation of plate-like morphology of $CuGaO_2$ particles from the sono-chemical method followed by firing at 850 °C with some agglomerations (Fig. 3a). The average size of the sub-micron sized plates was found to be in the range from 500 to 800 nm. Fig. 3b and c show the FESEM images of the hydrothermally synthesized nanocrystalline $CuGaO_2$ hexagons. The low and high magnification FESEM images reveal that the hydrothermally synthesized nanocrystalline $CuGaO_2$ particles have regular hexagonal shape with the average thickness of ~40 nm. TEM studies also show the formation of the polygons with six edges and six verticals with diameter of ~500 nm (Fig. 3d). With more careful visualization by TEM studies, these nanocrystalline $CuGaO_2$ hexagons appear to be composed of tiny nanoparticles with the average particle size of ~10 nm. Similar type of nanoparticle aggregations to sub-micron sized hexagonal plates from other materials have also been reported by micro-emulsion method [27]. Fig. 3e shows the formation of micron–sized spherical shaped particles of $CuGaO_2$ by the solid state method. Energy-dispersive X-ray spectroscopic (EDS) studies confirmed that these delafossite $CuGaO_2$ samples contained only copper, gallium and oxygen elements without any impurity which clearly support the PXRD patterns of these delafossite $CuGaO_2$ samples (Figs. 3f and 1). The elemental composition of the copper and gallium was found according to the initial 1:1 loading stoichiometry. The appearance of carbon content in the EDS studies is mainly due to the surface of carbon tape on sample holder (Fig. 3f). From the BET surface area measurements, the specific surface area of the nanocrystalline $CuGaO_2$ hexagons, sub-micron sized $CuGaO_2$ plates and micron-sized $CuGaO_2$ particles were found to be 2.63, 2.33 and 0.42 m^2/g, respectively. So the specific surface area per unit volume of $CuGaO_2$ particles decreases with increasing of particle size of $CuGaO_2$ as expected.

Thermal properties of all three delafossite $CuGaO_2$ samples, i.e. sub-micron sized plates, nanocrystalline hexagons and micro-sized particles, were investigated in oxygen atmosphere with the heating rate of 5 °C/min up to 800 °C using the Perkin-Elmer TGA analyzer. As shown in Fig. 4, a very small weight loss was initially observed that could be due to the adsorbed moisture, and then the thermal studies of the delafossite $CuGaO_2$ samples showed no weight loss/gain up to 350 °C in oxygen, which indicates the existence/absence of oxygen deficiency in the $CuGaO_2$ samples. The weight increase above 350 °C was attributed the decomposition of the $CuGaO_2$ sample. The weight gain was saturated to ~4.9% at 700 °C, which indicated that the decomposition of $CuGaO_2$ was completed to CuO and $CuGa_2O_4$ as also reported in the literature [23,24].

Cyclic voltammetry (CV) and chrono-amperometric (CA) measurements were carried out to test the OER and HER performance of these delafossite $CuGaO_2$ samples with different morphologies. For the electro-catalytic measurements, 0.5 M KOH and Ag/AgCl were used as the electrolyte and reference electrode, respectively, and N_2 gas was passed through the electrolyte for 5 min before the tests. Fig. 5a shows the CV curves of the nanocrystalline hexagons, sub-micron sized plates and micron-sized particles of delafossite $CuGaO_2$ from –1.0 to 1.1 V versus Ag/AgCl with the scan rate of 50 mV/s. Cyclic voltammograms demonstrate redox behavior around −0.2 V. A sharp peak was observed around −0.18 V, which is due to the oxidation of Cu^+ to Cu^{2+}, as reported in the literature [19]. This is noteworthy that the electro-catalytic oxidation current was observed in CV beyond the potential of 0.5 V to OER in 0.5 M KOH according to the following reaction occurs at anode: $4OH^- \rightarrow 2H_2O + 2O_2 + 4e^-$. From the CV curves, the nanocrystalline $CuGaO_2$ hexagons generate higher current than the sub-micron sized $CuGaO_2$ plates and micron-sized $CuGaO_2$ particles.

Chrono-amperometry (CA) is a potentiostatic true quantitative measurement to investigate the electro-catalytic behavior of the nanomaterials at the fixed potential with time. Fig. 5b shows the chrono-amperometric measurements of the nanocrystalline hexagons, sub-micron sized plates and micron-sized particles of $CuGaO_2$ at the fixed potential of 0.60 V for 250 s for OER. By comparing the catalytic activity of all four electrodes with CA, it is clearly observed that the nanocrystalline $CuGaO_2$ hexagons generate higher current than the sub-micron sized plates and micron-sized particles of $CuGaO_2$. It means that the nanocrystalline $CuGaO_2$ hexagons show higher electro-catalytic activity than the sub-micron and micron sized particles toward OER. No current is generated when we use an electrode without any electro-catalyst. The electrode without catalytic materials contains only carbon black and PVDF. A careful visualization shows that the current decreases with time using the sub-micron sized $CuGaO_2$ plates obtained via sono-chemical process as the catalysts while the generated current was more stable with time when the nanocrystalline $CuGaO_2$ hexagons obtained via hydrothermal process were used as the catalysts. This could be possible because of the degradation of the $CuGaO_2$ plates as the catalysts on oxidation. Therefore, the $CuGaO_2$ hexagons are more stable electro-catalytic materials compared to the other two samples.

The current density for the nanocrystalline $CuGaO_2$ hexagons, sub-micron sized plates and micron-sized particles was calculated by using the electro-active surface area of the electrode. The geometric electro-active surface area of electrodes for OER was calculated by using Randles–Sevcik equation [28–30] as that of the nanocrystalline hexagons is equal to 0.21 cm^2, that of the sub-micron sized plates to 0.19 cm^2, and that of the micron-sized particles to 0. 12 cm^2. Commonly, the current densities of the materials were calculated using the resulting currents obtained from the electrochemical measurements divided by the geometric electroactive surface area of the electrode. Therefore, the current densities of the nanocrystalline $CuGaO_2$ hexagons, sub-micron sized plates and micron-sized particles at 0.60 V were found to be

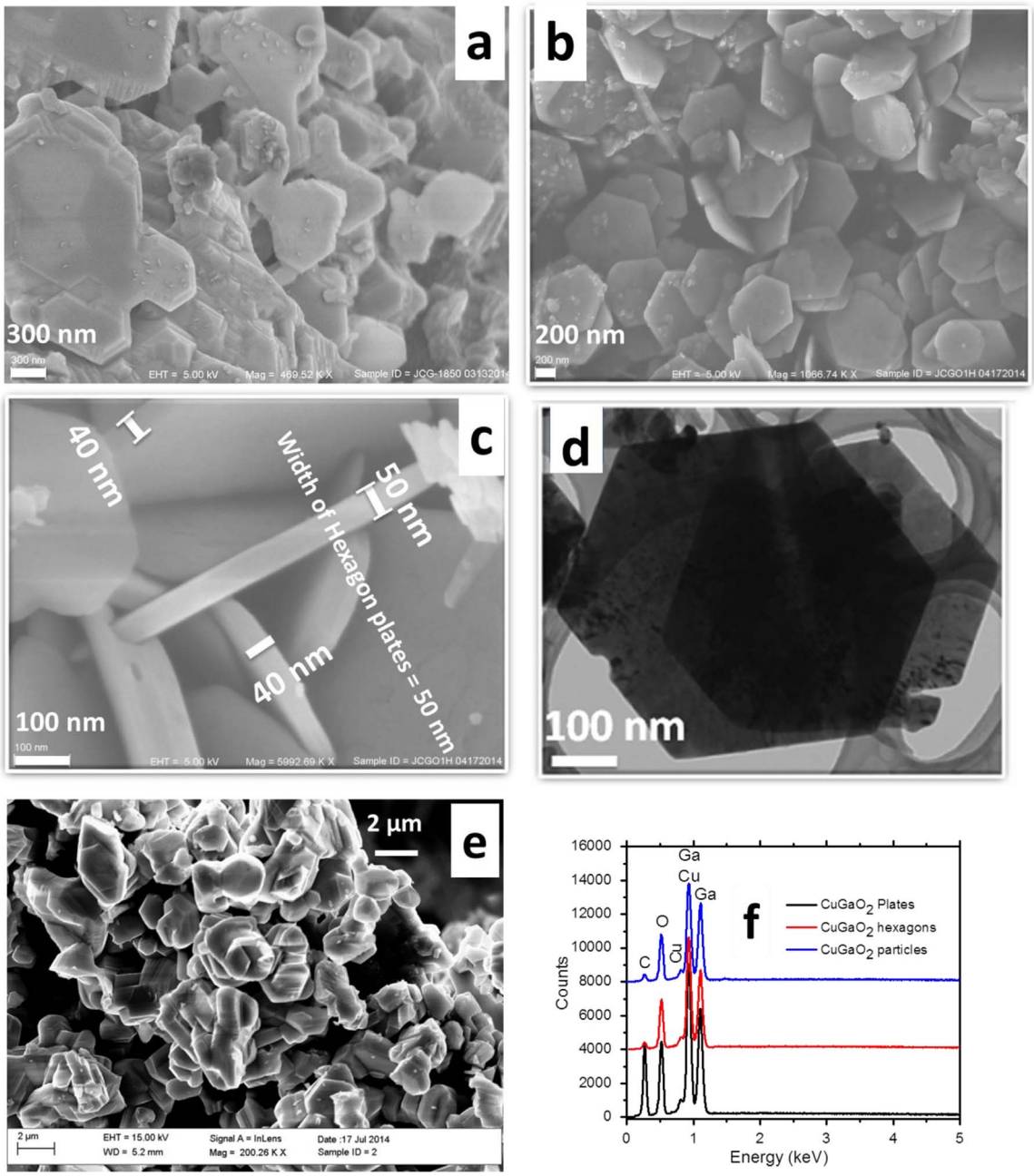

Fig. 3. (a) FESEM image of the sub-micron sized $CuGaO_2$ plates; (b) Low- and (c) high-magnification FESEM; (d) TEM images of the nanocrystalline $CuGaO_2$ hexagons; (e) FESEM image of the micron-sized $CuGaO_2$ particles; (f) EDS spectra of the nanocrystalline $CuGaO_2$ hexagons, sub-micron sized $CuGaO_2$ plates and micron-sized $CuGaO_2$ particles.

26, 23 and 5 mA/cm^2, respectively. So the current density of the nanocrystalline $CuGaO_2$ hexagons was found to be more than 5 times higher than the micron-sized $CuGaO_2$ particles while close to that of the sub-micron sized $CuGaO_2$ plates. To the best of our knowledge, there were very few reports in the literature on delafossite $CuRhO_2$, $CuGaO_2$, $CuFeO_2$, and $CuAlO_2$ micron-sized particles as the electro-catalysts for OER using 1.0 M KOH electrolyte and reversible hydrogen electrode as a reference electrode by applying the potential of 1.6 V [17]. Moreover, the nanocrystalline delafossite $CuGaO_2$ hexagons are an efficient electro-catalyst to OER at much lower potentials compared to the reported delafossite compounds [17]. Previously, the current density of $CuGaO_2$ particles for OER was reported to be ~8 mA/cm^2 at the applied potential of 1.6 V [17], while our results here showed that nanocrystalline $CuGaO_2$ hexagons and submicron sized plates generate much higher current densities of ~26 and ~23 mA/cm^2, respectively, at much lower applied potential, i.e. 0.60 V. Table 1 shows the comparison of the electro-catalytic performances of the as–synthesized delafossite $CuGaO_2$ nanostructures with those of previously reported delafossite compounds. These nanocrystalline hexagons and sub-micron sized plates of delafossite $CuGaO_2$ show higher current density than metallic copper nanoparticles (15 mA/cm^2 with Pt as a working electrode) [19], and copper (I) oxide nanostructures (20 mA/cm^2 with glassy carbon as a working electrode and 35.5 mA/cm^2 with Pt as a working electrode) versus Ag/AgCl [19]. Several other materials like IrO_2, RhO_2 are the important electro-catalysts for OER, but it is always prominent to find less expensive catalysts as alternates. The nanocrystalline $CuGaO_2$ hexagons also show much higher electro-catalytic activity than IrO_2 (~4 µA/cm^2 in acidic and ~2 µA/cm^2 in alkaline medium)

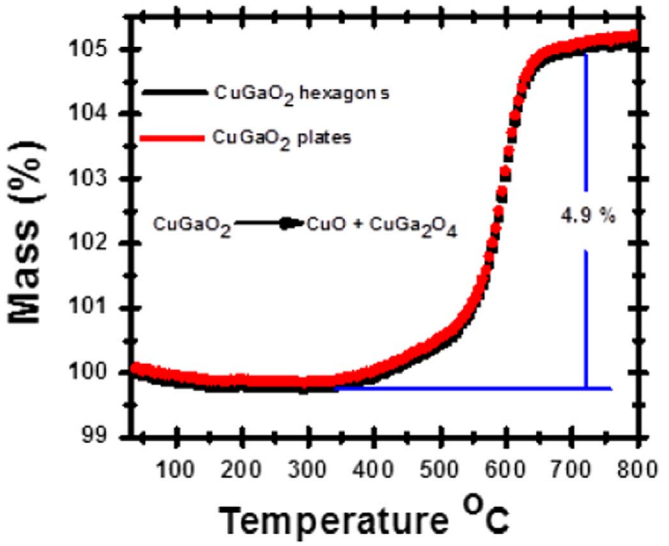

Fig. 4. TGA studies of the delafossite $CuGaO_2$ samples (nanocrystalline hexagons and sub-micron sized plates) in oxygen.

and RuO_2 ($\sim$10 μA/cm^2 in acidic and $\sim$3 μA/cm^2 in alkaline medium) at 1.48 V versus RHE [31]. The current density of IrO_2 nanoflowers was reported to be of 0.5 mA/cm^2 in 0.1 M buffer solution using glassy carbon electrode versus Ag/AgCl [32].

The current densities of the nanocrystalline $CuGaO_2$ hexagons, sub-micron sized plates and micron-sized particles were also calculated using the amount of materials pasted on electrode, observed current and BET surface area of the materials. The current densities for OER were found to be 0.099, 0.062 and 0.015 mA/cm^2 of nanocrystalline hexagons, sub-micron sized plates and micron-sized particles of $CuGaO_2$, respectively, at 0.60 V. The electro-catalytic performance of nanocrystalline $CuGaO_2$ hexagons for OER was found much higher (1.5 and 6 times) than the performances observed with sub-micron sized $CuGaO_2$ plates and micron-sized $CuGaO_2$ particles.

These delafossite $CuGaO_2$ samples have also been used as electro-catalysts for HER. CV curves show that the hydrogen evolution begins from -0.9 V versus Ag/AgCl electrode according to the following reaction: $2H_2O+2e^- \rightarrow H_2+2OH^-$ (Fig. 5a). During the electro-catalysis process, electrons transfer from the delafossite $CuGaO_2$ electrode materials to water molecules to generate H_2 and OH^-. Nanocystalline $CuGaO_2$ hexagons perform better electro-catalytic activity compared to the sub-micron sized $CuGaO_2$ plates and micron-sized particles to HER. CA studies of the delafossite $CuGaO_2$ particles were carried out to confirm the catalytic activity toward the evolution of hydrogen in 0.5 M KOH at -1.2 V for 250 s (Fig. 5c). By comparing the current density of all three electrode materials from CA, we clearly observe that the nanocrystalline hexagons generate higher current compared to the sub-micron sized plates and the micron-sized particles with time. The current densities of the nanocrystalline hexagons, sub-micron sized plates and micron-sized particles were found to be about 65, 45, and 35 mA/cm^2, respectively. The current density is directly proportional to the generation of oxygen or hydrogen which depends on both the surface area and the morphology of the catalysts. By using the BET surface area to compare the catalytic activities of all three electrodes, we examined that the nanocrystalline hexagons (0.25 mA/cm^2) show higher efficiency compared to the sub-micron sized plates (0.122 mA/cm^2) and the micron-sized particles (0.105 mA/cm^2). The current density obtained could be a function of both the faradaic and non-faradaic processes. The faradic process is the only one that contributes to either OER or HER by the illustration of charge being transferred with these

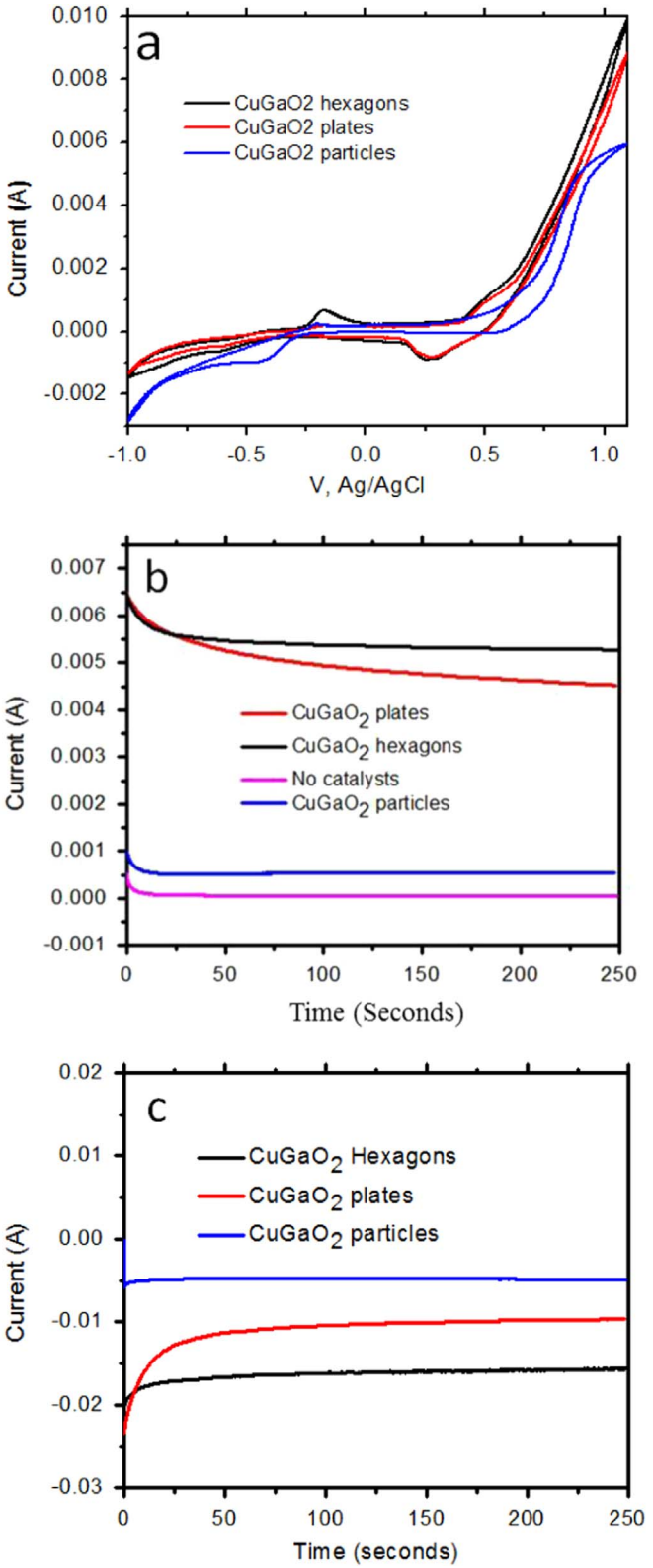

Fig. 5. (a) Cyclic voltammograms of the nanocrystalline $CuGaO_2$ hexagons, sub-micron sized $CuGaO_2$ plates and micron-sized $CuGaO_2$ particles in 0.5 M KOH by applying the potential range from –1.0 to 1.1 V vs Ag/AgCl with scan rate of 50 mV/s; (b) chronoamperometric voltammograms of the nanocrystalline $CuGaO_2$ hexagons, sub-micron sized $CuGaO_2$ plates and micron-sized $CuGaO_2$ particles for OER at 0.6 V for 250 s; (c) Chronoamperometric voltammograms of the nanocrystalline $CuGaO_2$ hexagons, sub-micron sized $CuGaO_2$ plates and micron-sized $CuGaO_2$ particles for HER at -1.2 V for 250 s. Note that N_2 gas was purged through the electrolyte for 5 min prior to the electrochemical measurements to remove dissolved air from the electrolyte.

Table 1
Comparison of the electro-catalytic activities of the as-synthesized delafossite $CuGaO_2$ nanostructures for OER with previous reports in the literature.

Samples	Applied potential (V)	Current density (mA/cm^2)	Ref. #
Nanocrystalline $CuGaO_2$ hexagons	0.60	26	Present study
$CuGaO_2$ sub-micron sized plates	0.60	23	Present study
$CuGaO_2$ micron-sized particles	0.60	5	Present study
$CuGaO_2$ micron-sized particles	1.6	6	17
$CuRhO_2$ micron-sized particles	1.6	8	17
$CuGaO_2$ micron-sized particles	2.0	30	17
$CuAlO_2$ micron-sized particles	2.0	10	17
$CuFeO_2$ micron-sized particles	2.0	8	17
$CuYO_2$ micron-sized particles	2.0	5	17

$CuGaO_2$ particles while the non-faradic process stimulates the formation of the electrical double layer. Note that here we reported that delafossite $CuGaO_2$ is also an efficient electro-catalyst for HER for the first time. The investigation of $CuGaO_2$ electro-catalysts for the generation of hydrogen is highly admirable as the next generation fuel.

By using the cyclic voltammetry, the freshly prepared electrodes of the nanocrystalline $CuGaO_2$ hexagons (Fig. 6a), sub-micron sized $CuGaO_2$ plates (Fig. 6b) and micron-sized $CuGaO_2$ particles (Fig. 6c) were also used to investigate the OER in O_2 saturated 0.5 M KOH by applying potential ranging from −0.60 to 0.80 V versus Ag/AgCl electrode. All the measurements were carried out at various scan rates of 10, 25, 50 mV/s. These delafossite $CuGaO_2$ samples start the current generation from 0.55 V and act as electro-catalysts for OER beyond this potential. From the CV curves, we observed that the peak current is higher for the nanocrystalline hexagons than the sub-micron sized plates and micron-sized particles at 0.8 V versus Ag/AgCl (Figs. 6a–c). The peak current is directly proportional to the amount of oxygen evolved during the electrolysis which depends on the surface area and morphology of the electro-catalysts.

The electro-catalytic activities of these nanocrystalline hexagons, sub-micron sized plates and micron-sized particles of delafossite $CuGaO_2$ were also investigated by chrono-amperometric measurements in O_2 saturated 0.5 M KOH at 0.60 V for 200 s (Fig. 6d). In the chrono-amperometric experiments, the chemical reaction occurred on the surface of working electrode to generate the current during the electrolysis at the applied voltage of 0.60 V versus Ag/AgCl and the electrochemical reaction stops when the potential is switched off and hence current drops to zero.

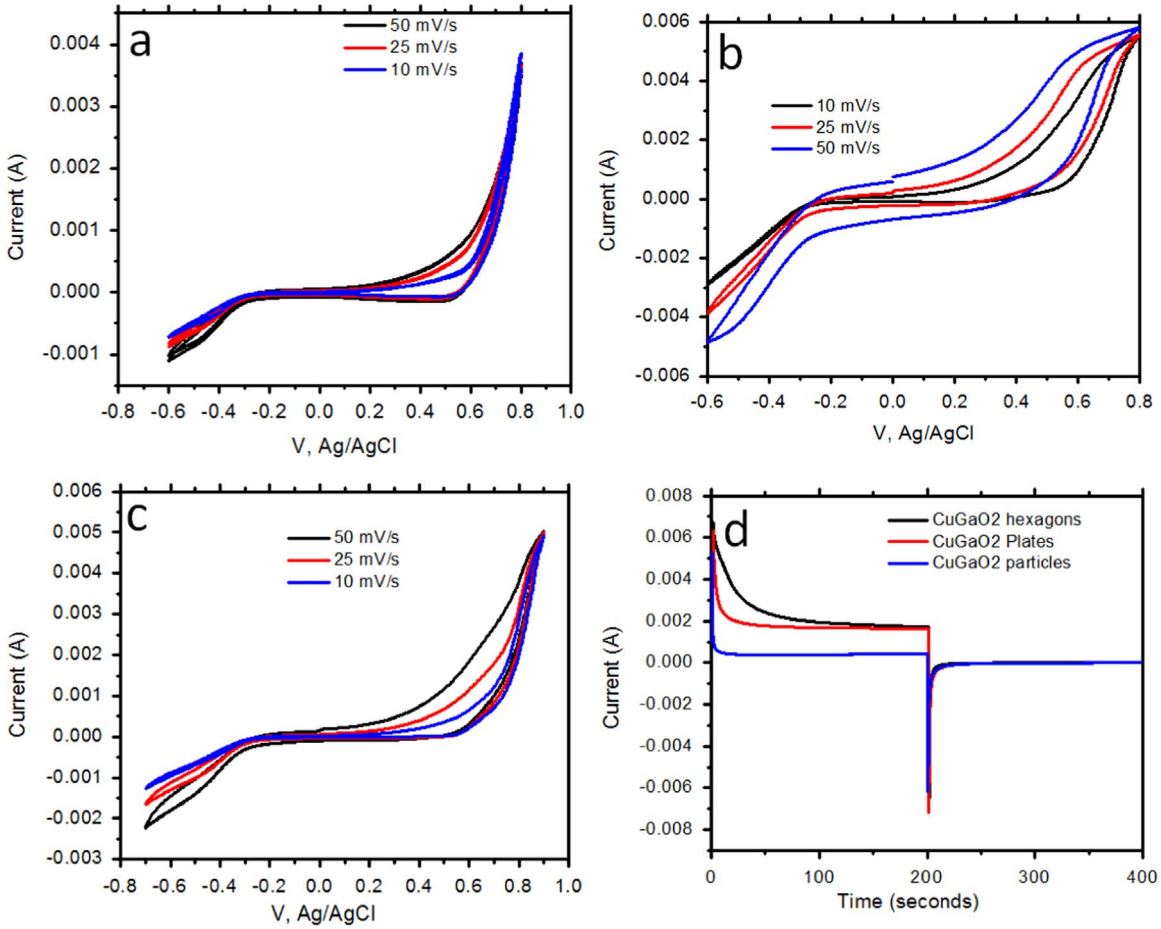

Fig. 6. Cyclic voltammograms of the (a) nanocrystalline $CuGaO_2$ hexagons; (b) sub-micron sized $CuGaO_2$ plates; (c) micron-sized $CuGaO_2$ particles for OER in saturated O_2 and 0.5 M KOH using various scan rates, i.e. 10, 25, and 50 mV/s;. (d) Chronoamperometric voltammograms of the nanocrystalline $CuGaO_2$ hexagons, sub-micron sized $CuGaO_2$ plates and micron-sized $CuGaO_2$ particles for OER in saturated O_2 and 0.5 M KOH.

Calculated by using the Randles–Sevcik equation, the geometric electro-active surface area of the electrodes was found to be 0.09, 0.126 and 0.085 cm^2 of the nanocrystalline $CuGaO_2$ hexagons, sub-micron sized $CuGaO_2$ plates and micron-sized $CuGaO_2$ particles, respectively [28–30]. By comparing the electro-catalytic activity of the nanocrystalline $CuGaO_2$ hexagons, sub-micron sized plates, and micron-sized particles for OER, it was clearly observed again that the nanocrystalline hexagons (20 mA/cm^2) possess better catalytic activity than the sub-micron sized plates (12 mA/cm^2) and micron-sized particles (5 mA/cm^2) at 0.6 V versus Ag/AgCl. Recently, Stoerzinger et al. have reported the orientation dependent oxygen evolution activity of IrO_2 nanocrystals (3 $\mu A/cm^2$ for $<100>$ and 0.5 $\mu A/cm^2$ for $<110>$) in O_2–saturated 0.1 M KOH at 1.2 V versus RHE [33]. Hence, the nanocrystalline $CuGaO_2$ hexagons show enhanced electro-catalytic behavior than the most active IrO_2 electrode materials in oxygen saturated electrolyte at 0.6 V versus Ag/AgCl. For OER, the current densities were also calculated using the BET surface area. The current densities were found to be 0.033, 0.021 and 0.011 of the nanocrystalline $CuGaO_2$ hexagons, sub-micron sized $CuGaO_2$ plates and micron-sized $CuGaO_2$ particles, respectively. Therefore, oxygen evolution efficiency of the nanocrystalline $CuGaO_2$ hexagons is much better than the sub-micron sized $CuGaO_2$ plates and micron-sized $CuGaO_2$ particles. The observed current is proportional to the amount of oxygen or hydrogen generated during the electrolysis of water. The amount of current generation is a function of surface area, size and morphology of nanomaterials. The specific surface area (from BET) of the nanocrystalline $CuGaO_2$ hexagons was found to be higher (2.63 m^2/g) compared to the sub-micron sized $CuGaO_2$ plates (2.33 m^2/g) and micron-sized $CuGaO_2$ particles (0.42 m^2/g), which also support the observed electrolysis of water to OER and HER.

4. Conclusions

In the present study, we tested and compared a type of active and cost effective electrode material, i.e. delafossite $CuGaO_2$ with three different morphologies, for the electrolysis of water to sustain the efficiency in fuel generation technology. The phase purity and morphology of the synthesized materials were confirmed from the PXRD, Raman spectroscopy, and electron microscopic studies. The nanocrystalline $CuGaO_2$ hexagons show superior electro-catalytic activity than the sub-micron sized plates and micron sized particles of $CuGaO_2$ toward oxygen and hydrogen evolution reactions in both nitrogen- and oxygen-saturated 0.5 M KOH electrolyte versus Ag/AgCl. Therefore, it is expected that these delafossite $CuGaO_2$ particles could be useful for sustainable energy conversion applications.

Acknowledgments

The authors thank the support from the American Chemical Society – Petroleum Research Fund #51497, the Air Force Office of Scientific Research (award # FA9550-12-1-0159), and the National Science Foundation under DMR Grant # 0934157 (PREM-UTPA/UMN-Science and Engineering of Polymeric and Nanoparticle-based Materials for Electronic and Structural Applications). J.A. is gratefully acknowledged "The Deanship of Scientific Research, Research Center, College of Science, King Saud University, Kingdom of Saudi Arabia". The authors also thank Mr. Q. Li for taking SEM images, Ms. T. Olmedo for taking TEM images, Dr. M. Pokhrel for EDX studies, and Ms. J. Cruz for performing BET measurements.

References

[1] R. Srinivasan, B. Chavillon, C. Doussier-Brochard, L. Cario, M. Paris, E. Gautron, P. Deniard, F. Odobel, S. Jobic, Tuning the size and color of the *p*-type wide band gap delafossite semiconductor $CuGaO_2$ with ethylene glycol assisted hydrothermal synthesis, J. Mater. Chem. 18 (46) (2008) 5647–5653.
[2] M. Yu, G. Natu, Z. Ji, Y. Wu, *p*-type dye-sensitized solar cells based on delafossite $CuGaO_2$ nanoplates with saturation photovoltages exceeding 460 mV, J. Phys. Chem. Lett. 3 (9) (2012) 1074–1078.
[3] Z. Xu, D. Xiong, H. Wang, W. Zhang, X. Zeng, L. Ming, W. Chen, X. Xu, J. Cui, M. Wang, S. Powar, U. Bach, Y.-B. Cheng, Remarkable photocurrent of *p*-type dye-sensitized solar cell achieved by size controlled $CuGaO_2$ nanoplates, J. Mater. Chem. A 2 (9) (2014) 2968–2976.
[4] J. Li, A.W. Sleight, C.Y. Jones, B.H. Toby, Trends in negative thermal expansion behavior for AMO_2 (A=Cu or Ag; M=Al, Sc, In, or La) compounds with the delafossite structure, J. Solid State Chem. 178 (1) (2005) 285–294.
[5] M. John, S. Heuss-Aßbichler, S. Park, A. Ullrich, G. Benka, N. Petersen, D. Rettenwander, S.R. Horn, Low-temperature synthesis of $CuFeO_2$ (delafossite) at 70 °C: a new process solely by precipitation and ageing, J. Solid State Chem. 233 (2016) 390–396.
[6] X. Nie, S.-H. Wei, S.B. Zhang, Bipolar doping and band-gap anomalies in delafossite transparent conductive oxides, Phys. Rev. Lett. 88 (6) (2002) 066405.
[7] J. Robertson, P.W. Peacock, M.D. Towler, R. Needs, Electronic structure of *p*-type conducting transparent oxides, Thin Solid Films 411 (1) (2002) 96–100.
[8] H. Kawazoe, M. Yasukawa, H. Hyodo, M. Kurita, H. Yanagi, H. Hosono, *P*-type electrical conduction in transparent thin films of $CuAlO_2$, Nature 389 (6654) (1997) 939–942.
[9] M.J. Han, T. Huang, J.Z. Zhang, Y.W. Li, G. Hu, Structural, optical and electrical properties of delafossite $CuGaO_2$ films grown by sol-gel method, Proc. SPIE (2013) 906809, http://dx.doi.org/10.1117/12.2053125.
[10] T. Omata, H. Nagatani, I. Suzuki, M. Kita, H. Yanagi, N. Ohashi, Wurtzite $CuGaO_2$: a new direct and narrow band gap oxide semiconductor applicable as a solar cell absorber, J. Am. Chem. Soc. 136 (9) (2014) 3378–3381.
[11] A. Renaud, B. Chavillon, L. Le Pleux, Y. Pellegrin, E. Blart, M. Boujtita, T. Pauporte, L. Cario, S. Jobic, F. Odobel, $CuGaO_2$: a promising alternative for NiO in *p*-type dye solar cells, J. Mater. Chem. 22 (29) (2012) 14353–14356.
[12] K. Gurunathan, J.-O. Baeg, S.M. Lee, E. Subramanian, S.-J. Moon, K.-J. Kong, Visible light assisted highly efficient hydrogen production from H_2S decomposition by $CuGaO_2$ and $CuGa_{1-x}In_xO_2$ delafossite oxides bearing nanostructured co-catalysts, Catal. Commun. 9 (3) (2008) 395–402.
[13] J.W. Lekse, M.K. Underwood, J.P. Lewis, C. Matranga, Synthesis, characterization, electronic structure, and photocatalytic behavior of $CuGaO_2$ and $CuGa_{1-x}Fe_xO_2$ (x=0.05, 0.10, 0.15, 0.20) delafossites, J. Phys. Chem. C 116 (2) (2011) 1865–1872.
[14] I. Herraiz-Cardona, F. Fabregat-Santiago, A. Renaud, B. Julián-López, F. Odobel, L. Cario, S. Jobic, S. Giménez, Hole conductivity and acceptor density of *p*-type $CuGaO_2$ nanoparticles determined by impedance spectroscopy: the effect of Mg doping, Electrochim. Acta 113 (2013) 570–574.
[15] P.F. Carcia, R.D. Shannon, P.E. Bierstedt, R.B. Flippen, O_2 electrocatalysis on thin film metallic oxide electrodes with the delafossite structure, J. Electrochem. Soc. 127 (9) (1980) 1974–1978.
[16] R. Hinogami, K. Toyoda, M. Aizawa, T. Kawasaki, H. Gyoten, Copper delafossite anode for water electrolysis, ECS Trans. 58 (2) (2013) 27–31.
[17] R. Hinogami, K. Toyoda, M. Aizawa, S. Yoshii, T. Kawasaki, H. Gyoten, Active copper delafossite anode for oxygen evolution reaction, Electrochem. Commun. 35 (2013) 142–145.
[18] J. Ahmed, Y. Mao, Delafossite $CuAlO_2$ nanoparticles with electrocatalytic activity toward oxygen and hydrogen evolution reactions, in: Jingbo Louise Liu, Sajid Bashir (Eds.), Nanomaterials for Sustainable Energy (Chpater 4), American Chemical Society, Washington DC, 2015, pp. 57–72.
[19] B. Kumar, S. Saha, A. Ganguly, A.K. Ganguli, A facile low temperature (350 °C) synthesis of Cu_2O nanoparticles and their electrocatalytic and photocatalytic properties, RSC Adv. 4 (23) (2014) 12043–12049.
[20] J. Ahmed, P. Trinh, A.M. Mugweru, A.K. Ganguli, Self-assembly of copper nanoparticles (cubes, rods and spherical nanostructures): significant role of morphology on hydrogen and oxygen evolution efficiencies, Solid State Sci. 13 (5) (2011) 855–861.
[21] J. Ahmed, A. Ganguly, S. Saha, G. Gupta, P. Trinh, A.M. Mugweru, S.E. Lofland, K. V. Ramanujachary, A.K. Ganguli, Enhanced electrocatalytic activity of copper–cobalt nanostructures, J. Phys. Chem. C 115 (30) (2011) 14526–14533.
[22] P. Melnikov, V.A. Nascimento, L.Z. Zanoni Consolo, Thermal decomposition of gallium nitrate hydrate and modeling of thermolysis products, J. Therm. Anal. Calorim. 107 (3) (2012) 1117–1121.
[23] Y. Kumekawa, M. Hirai, Y. Kobayashi, S. Endoh, E. Oikawa, T. Hashimoto, Evaluation of thermodynamic and kinetic stability of $CuAlO_2$ and $CuGaO_2$, J. Therm. Anal. Calorim. 99 (1) (2010) 57–63.
[24] A.P. Amrute, Z. Łodziana, C. Mondelli, F. Krumeich, J. Pérez-Ramírez, Solid-state chemistry of cuprous delafossites: synthesis and stability aspects, Chem. Mater. 25 (21) (2013) 4423–4435.
[25] M. Han, K. Jiang, J. Zhang, W. Yu, Y. Li, Z. Hu, J. Chu, Structural, electronic band transition and optoelectronic properties of delafossite $CuGa_{1-x}Cr_xO_2$ ($0 \le x \le 1$) solid solution films grown by the sol-gel method, J. Mater. Chem. 22 (35) (2012) 18463–18470.
[26] J. Pellicer-Porres, A. Segura, E. Martínez, A.M. Saitta, A. Polian, J.C. Chervin, B. Canny, Vibrational properties of delafossite $CuGaO_2$ at ambient and high

pressures, Phys. Rev. B 72 (6) (2005) 064301.
[27] J. Ahmed, Menaka, A.K. Ganguli, Controlled growth of nanocrystalline rods, hexagonal plates and spherical particles of the vaterite form of calcium carbonate, CrystEngComm 11 (5) (2009) 927–932.
[28] I. Taurino, S. Carrara, M. Giorcelli, A. Tagliaferro, G. De Micheli, Comparison of two different carbon nanotube-based surfaces with respect to potassium ferricyanide electrochemistry, Surf. Sci. 606 (3–4) (2012) 156–160.
[29] S. Min-Jung, Y. Dong-Hwa, J. Joon-Hyung, M. Nam-Ki, H. Suk-In, Comparison of effective working electrode areas on planar and porous silicon substrates for cholesterol biosensor, Jpn. J. Appl. Phys. 45 (9R) (2006) 7197.
[30] A.A.A. Aljabali, J.E. Barclay, J.N. Butt, G.P. Lomonossoff, D.J. Evans, Redox-active ferrocene-modified Cowpea mosaic virus nanoparticles, Dalton Trans. 39 (32) (2010) 7569–7574.
[31] Y. Lee, J. Suntivich, K.J. May, E.E. Perry, Y. Shao-Horn, Synthesis and activities of rutile IrO_2 and RuO_2 nanoparticles for oxygen evolution in acid and alkaline solutions, J. Phys. Chem. Lett. 3 (3) (2012) 399–404.
[32] C. Zhao, Y. E, L. Fan, Enhanced electrochemical evolution of oxygen by using nanoflowers made from a gold and iridium oxide composite, Microchim. Acta, 178, (2012) 107–114.
[33] K.A. Stoerzinger, L. Qiao, M.D. Biegalski, Y. Shao-Horn, Orientation-dependent oxygen evolution activities of rutile IrO_2 and RuO_2, J. Phys. Chem. Lett. 5 (10) (2014) 1636–1641.